2021

A geometric description of the set of stabilizing PID controllers

Keqin Gu
Southern Illinois University Edwardsville, kgu@siue.edu

Qian Ma
Nanjing University of Science and Technology, qianmashine@gmail.com

Huiqing Zhou
Southern Illinois University Edwardsville

Mahzoon Salma
University of Oklahoma

Xingzi Yang
University of Texas at San Antonio

Received: 29 November 2020 | Accepted: 19 January 2021

DOI: 10.1002/rnc.5443

SPECIAL ISSUE ARTICLE

WILEY

A geometric description of the set of stabilizing PID controllers

Keqin Gu[1] | **Qian Ma**[2] | **Huiqing Zhou**[1] | **Salma Mahzoon**[3] | **Xingzi Yang**[4]

[1]Department of Mechanical and Industrial Engineering, Southern Illinois University Edwardsville, Edwardsville, Illinois, USA

[2]School of Automation, Nanjing University of Science and Technology, Nanjing, China

[3]School of Aerospace and Mechanical, University of Oklahoma, Norman, Oklahoma, USA

[4]Department of Mechanical Engineering, University of Texas at San Antonio, San Antonio, Texas, USA

Correspondence
Qian Ma, School of Automation, Nanjing University of Science and Technology, Nanjing 210094, China.
Email: qianmashine@gmail.com

Abstract

This article developed a new method to described the set of stabilizing PID control. The method is based on D-parameterization with natural description of the set. It was found that the stability crossing surface is a ruled surface that is completely determined by a curve known as discriminant. The discriminant is divided into sectors at the cusps. Corresponding to the sectors, the stability crossing surface is divided into positive and negative patches. A systematic study is conducted to identify the regions with a fixed number of right half-plane characteristic roots. The crossing directions of characteristic roots for positive patches and negative patches are also studied. As a result, a systematic method is developed to identify the regions of PID parameter such that the system is stabilized.

KEYWORDS

geometric characterization, PID control, stability

1 | INTRODUCTION

As PID control is widely used in industrial applications, it is natural that a substantial amount of research has been conducted on the tuning of PID-type of control.[1-5] are some examples.

However, the control objectives for different systems may be different, and it is often necessary to consider trade-offs between different performance specifications to reach reasonable compromise.[6] In such a situation, it is valuable to first identify the set of all PID parameters that stabilizes the system. Obviously, the performance specifications are meaningful only when the PID parameters are restricted to within this set. The first description of such stabilizing set has been achieved using the Hermite–Biehler theorem.[7] It was found that the intersection of the stabilizing parameter set with a fixed proportional gain plane consists of polygons, and a linear programming method may be used to facilitate identifying the stabilizing set.[8,9] Additional results along this line have been obtained using other methods or introducing additional concepts. For example, Nyquist plot was used in Reference 6, and singular frequency concept was introduced in Reference 10. A more explicit description has been achieved for a second-order system in Reference 11. To summarize, the methods in most currently available literature try to visualize the stabilizing set through its cross-section with a constant proportional gain. While such cross sections have a very simple geometric structure of polygons, it is not easy to obtain a global view of the entire stabilizing set.

In this article, we present a more natural description of the geometric structure of the stabilizing set. With the proportional gain as the vertical axis in the three-dimensional parameter space, we visualize the set by projecting it to the horizontal plane. This bird-eye view allows us to see directly all the regions in the horizontal plane where there exist proportional gains to stabilize the system. The method is based on the D-parameterization. Roughly speaking, the stability

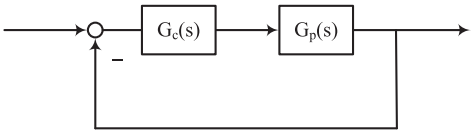

FIGURE 1 The plant of closed-loop system

crossing surface, which consists of parameters such that at least one characteristic root is on the imaginary axis, is described. This stability crossing surface partition the three-dimensional parameter space into regions of constant number of right half-plane (RHP) characteristic roots. Especially, the regions where there is no RHP characteristic root are identified and declared as the set of stabilizing PID parameters.

Our study has discovered a number of very useful properties of the stability crossing surface to facilitate a systematic process of identifying all the stabilizing regions in the parameter space. It is observed that the stability crossing surface is a ruled surface consisting of horizontal straight lines. This ruled surface is completely determined by its discriminant, which is the curve on the surface consisting of the points with vertical tangent planes. The stability crossing surface may be divided into a number of positive and negative patches with the cusps of the discriminant (when projected to the horizontal plane) as the dividing points. The crossing directions of the characteristic roots are the same for all the positive patches as the proportional gain increases, and it is opposite to those corresponding to the negative patches.

The article is organized as follows. Section 2 formulates the stability crossing surface. Section 3 introduces discriminant. Section 4 describes cusps and patches. Sections 5 and 6 are devoted to relative vertical positions of patches and crossing directions. Section 7 presents some conclusions. A preliminary version of this article was presented in Reference 12.

2 | STABILITY CROSSING SURFACE

For a given a plant with transfer function $G_p(s)$, we want to determine the set of coefficients (k_d, k_i, k_p) of PID controller

$$G_c(s) = k_p + \frac{k_i}{s} + k_d s, \tag{1}$$

such that the closed-loop system shown in Figure 1 is stable, that is, all the solutions of the system characteristic equation

$$\Delta(s) = 1 + G_c(s)G_p(s) = 0, \tag{2}$$

are on the left half-plane (LHP). For this purpose, it is instrumental to introduce the following concept of stability crossing surface.

Definition 1. The set of all $(k_d, k_i, k_p) \in \mathbb{R}^3$ such that the characteristic equation $\Delta(s) = 0$ has at least one solution on the imaginary axis is known as the stability crossing surface, and is denoted as $\mathcal{K}$.

In order to focus on the main idea, we make the following assumption about the plant transfer function.

Assumption 1. The transfer function can be written as $G_p(s) = N_p(s)/D_p(s)$, where $N_p(s)$ and $D_p(s)$ are polynomials with real coefficients. Furthermore, neither $N_p(s)$ nor $D_p(j\omega)$ has any roots on the imaginary axis.

Cases that violate the above assumption are not difficult to handle individually based on the principles presented in this article, but will not be pursued here.

Under Assumption 1, we may let $s = j\omega$ and multiply Equation (2) by $\frac{j\omega}{G_p(j\omega)}$ to obtain

$$\delta(j\omega) = \frac{j\omega}{G_p(j\omega)} + j\omega k_p + k_i - \omega^2 k_d = 0. \tag{3}$$

Therefore, the stability crossing surface $\mathcal{K}$ also corresponds to the solution of Equation (3) with real ω. Let the k_p-axis be the vertical axis in the (k_d, k_i, k_p) parameter space. Then, For $\omega = 0$, we obtain from the equation (3)

$$k_i = 0, \tag{4}$$

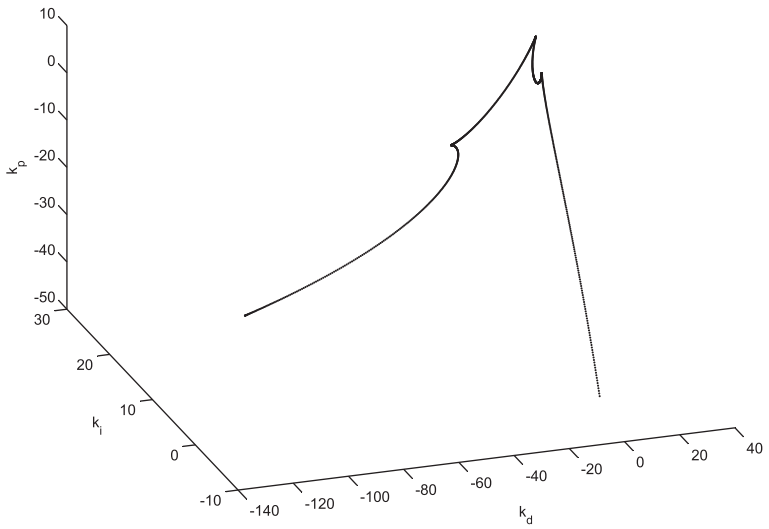

FIGURE 2 Discriminant of the ruled surface of system (10)

which is a vertical plane. For a fix $\omega \neq 0$, Equation (3) defines a horizontal straight line that can be described by the parametric equations

$$k_i = \omega^2 k_d - a(\omega), \tag{5}$$

$$k_p = -\frac{b(\omega)}{\omega}, \tag{6}$$

where

$$a(\omega) = \mathrm{Re}\left[\frac{j\omega}{G_p(j\omega)}\right], \tag{7}$$

$$b(\omega) = \mathrm{Im}\left[\frac{j\omega}{G_p(j\omega)}\right]. \tag{8}$$

As the straight line depends on ω, we will denote it as $\mathcal{L}(\omega)$. The projection of this straight line on the (k_d, k_i) horizontal plane is described by (5), and is denoted as $\mathcal{PL}(\omega)$. Obviously, the slope of $\mathcal{PL}(\omega)$ is ω^2.

As the plant transfer function satisfies

$$G_p(j\omega) = G_p^*(-j\omega),$$

it is obvious that $a(\omega)$ is an even function of ω, and $b(\omega)$ is an odd function of ω. Therefore, $\mathcal{L}(\omega) = \mathcal{L}(-\omega)$. It is thus sufficient to restrict ω to $[0, \infty)$.

As ω varies from 0^+ to $+\infty$, the straight lines $\mathcal{L}(\omega)$ described by (5) and (6) form a surface, which we denote as $\mathcal{S}$,

$$\mathcal{S} = \bigcup_{\omega>0} \mathcal{L}(\omega).$$

Such a surface is known as a ruled surface.[13] The surface $\mathcal{S}$ may be parameterized by k_d and ω. The stability crossing surface $\mathcal{K}$ consists of this ruled surface $\mathcal{S}$ and the vertical plane described by (4) (which we will denote as $\mathcal{V}$). In general, barring some degenerate cases, as the parameter (k_d, k_i, k_p) crosses $\mathcal{S}$ at a point on $\mathcal{L}(\omega)$ for some $\omega \neq 0$, a pair of characteristic roots crosses the imaginary axis at $\pm j\omega$. If the parameter crosses the vertical surface $\mathcal{V}$, then one characteristic root crosses the imaginary axis at the origin.

As the vertical plane $\mathcal{V}$ is rather simple, we will spend most effort in understanding $\mathcal{S}$. Using the vector notation, a point in the parameter space may be expressed as

$$\mathbf{r} = k_d\mathbf{i} + k_i\mathbf{j} + k_p\mathbf{k},$$

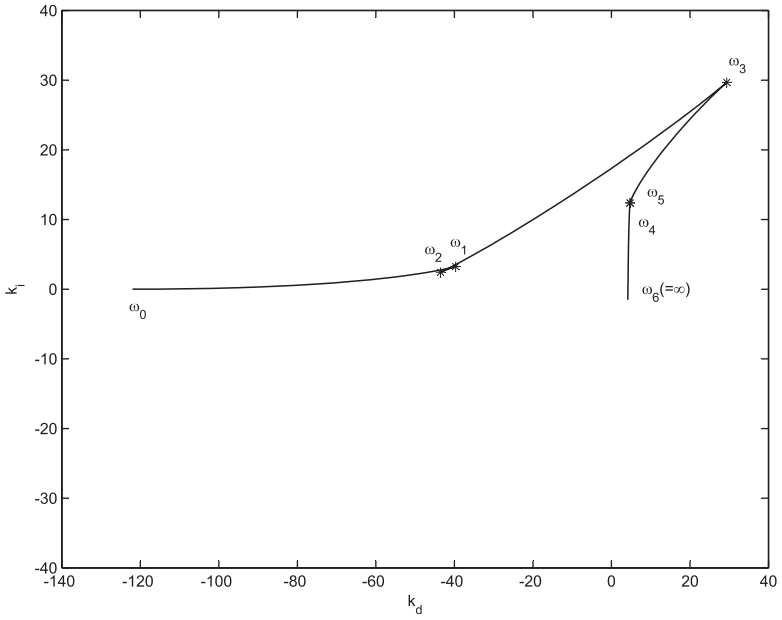

FIGURE 3 The projection of discriminant $\mathcal{PD}$ with cusps ω_i, $i = 1, 2, \ldots 5$

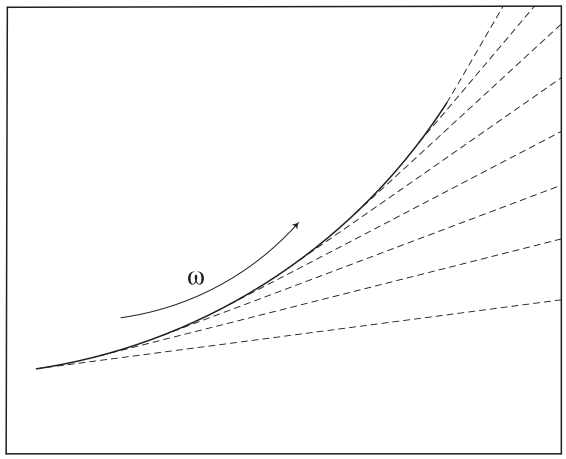

FIGURE 4 Illustration of $\mathcal{PS}_i^+$

Then, $\mathcal{S}$ can be written as

$$\mathbf{r} = \mathbf{r}(k_d, \omega), \tag{9}$$

with the components as functions of k_d and ω given by $k_d = k_d$ and (5) and (6). We will use the following plant transfer function, which was analyzed in Reference 10, to illustrate our description of $\mathcal{S}$ and stability analysis in the remaining part of this article

$$G_p(s) = \frac{-s^4 - 7s^3 - 2s + 1}{(s+1)(s+2)(s+3)(s+4)(s^2+s+1)}. \tag{10}$$

3 | DISCRIMINANT

In this section, we introduce the discriminant of the stability crossing surface $\mathcal{S}$. As will be demonstrated later, $\mathcal{S}$ is completely determined by the discriminant.

Definition 2. The discriminant of the ruled surface $\mathcal{S}$ described by (5) and (6) is a curve formed by the points on $\mathcal{S}$ with vertical tangent planes.

FIGURE 5 Illustration of $\mathcal{PS}_i^-$

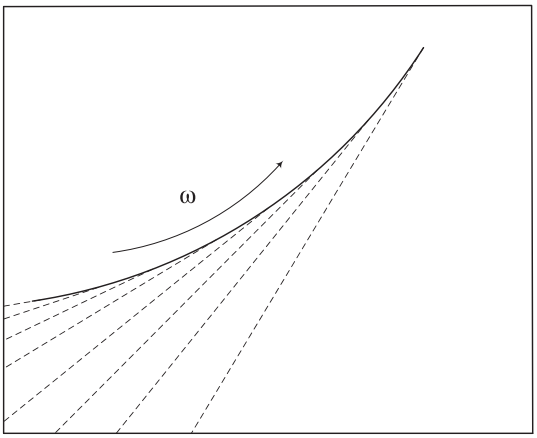

FIGURE 6 Division with $\mathcal{PD}_i$, $\mathcal{PL}^+(\omega_{i-1})$ and $\mathcal{PL}^+(\omega_i)$

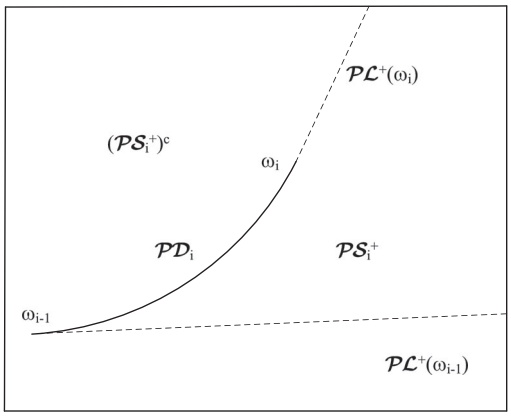

FIGURE 7 Division with $\mathcal{PD}_i$, $\mathcal{PL}^-(\omega_{i-1})$, and $\mathcal{PL}^-(\omega_i)$

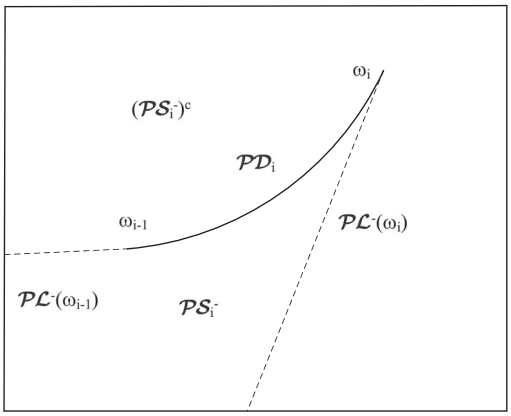

We will use $\mathcal{D}$ to denote the discriminant. With $\mathcal{S}$ described by (9), $\frac{\partial \mathbf{r}_S}{\partial k_d}$ and $\frac{\partial \mathbf{r}_S}{\partial \omega}$ are the two tangents of the curves formed by fixing either ω or k_d, respectively. The cross product of $\frac{\partial \mathbf{r}_S}{\partial k_d}$ and $\frac{\partial \mathbf{r}_S}{\partial \omega}$ is the normal vector to $\mathcal{S}$. Therefore, a point on $\mathcal{S}$ with vertical tangent plane satisfies

$$\left(\frac{\partial \mathbf{r}_S}{\partial k_d} \times \frac{\partial \mathbf{r}_S}{\partial \omega}\right) \cdot \mathbf{k} = 0, \tag{11}$$

where $\times$ is the cross product. Using the component expression, the above reduces to

$$\left(\frac{\partial k_i}{\partial \omega}\mathbf{k} - \frac{\partial k_p}{\partial \omega}\mathbf{j} + \omega^2 \frac{\partial k_p}{\partial \omega}\mathbf{i}\right) \cdot \mathbf{k} = 0. \tag{12}$$

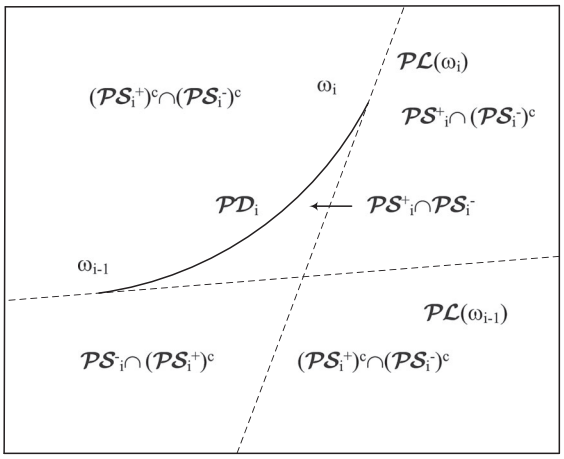

FIGURE 8 Division with $\mathcal{PD}_i$, $\mathcal{PL}(\omega_{i-1})$, and $\mathcal{PL}(\omega_i)$

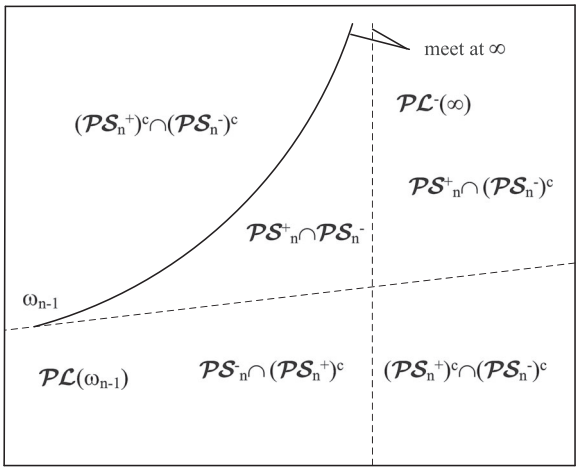

FIGURE 9 Division with $\mathcal{PD}_n$, $\mathcal{PL}(\omega_{n-1})$, and $\mathcal{PL}^-(\infty)$

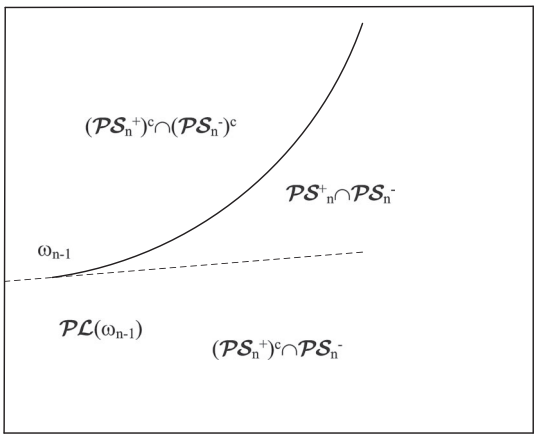

FIGURE 10 Division with $\mathcal{PD}_n$ and $\mathcal{PL}(\omega_{n-1})$

Using (5) in the above equation yields

$$2\omega k_d - a'(\omega) = 0, \tag{13}$$

which can be solved for k_d to obtain

$$k_d = \frac{a'(\omega)}{2\omega}. \tag{14}$$

FIGURE 11 The regions

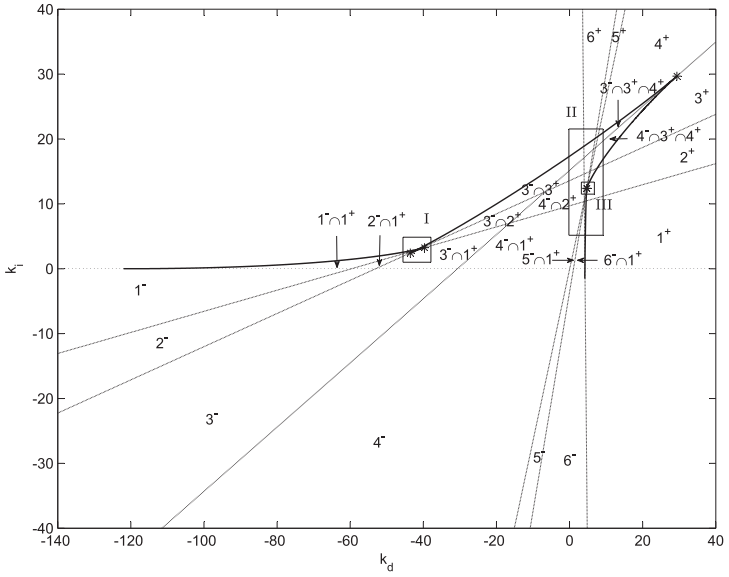

A substitution of (5) by (14) yields

$$k_i = \frac{1}{2}\omega a'(\omega) - a(\omega). \tag{15}$$

Therefore, the discriminant $\mathcal{D}$ is a curve that can be expressed as

$$\mathbf{r} = \mathbf{r}^d(\omega), \tag{16}$$

with the component form

$$k_d = k_d^d(\omega) = \frac{a'(\omega)}{2\omega}, \tag{17}$$

$$k_i = k_i^d(\omega) = \frac{1}{2}\omega a'(\omega) - a(\omega), \tag{18}$$

$$k_p = k_p^d(\omega) = -\frac{b(\omega)}{\omega}. \tag{19}$$

The discriminant of the system with plant transfer function (10) is shown in Figure 2.

It is instrumental to represent discriminant $\mathcal{D}$ by its projection to the horizontal plane and its vertical component as a function of ω. The horizontal projection is denoted as $\mathcal{PD}$, and is described by (17) and (18). For the system with plant transfer function (10), $\mathcal{PD}$ is plotted in Figure 3, and the k_p versus ω plot is given in Figure 15.

A critical observation is that $\mathcal{PD}$ is the envelope of the family of straight lines $\mathcal{PL}(\omega)$. This can be shown as follows. $\mathcal{PD}$ can be expressed as (17) and (18). Define $\phi(\omega) = \omega a'' - a'(\omega)$. Taking the derivative of (17) and (18), we obtain

$$(k_d^d)'(\omega) = \frac{\omega a'' - a'(\omega)}{2\omega^2} = \frac{\phi(\omega)}{2\omega^2}, \tag{20}$$

$$(k_i^d)'(\omega) = \frac{\omega a'' - a'(\omega)}{2} = \frac{\phi(\omega)}{2}. \tag{21}$$

When

$$\phi(\omega) \neq 0, \tag{22}$$

the slope of the tangent of $\mathcal{PD}$ at ω is ω^2, which is identical to $\mathcal{PL}(\omega)$. It is also obvious that $k_d^d(\omega)$ and $k_i^d(\omega)$ satisfies (5), which indicates that this point in $\mathcal{PD}$ belongs to the straight line $\mathcal{PL}(\omega)$. This allows us to conclude that the tangent of $\mathcal{PD}$ at ω indeed coincides with $\mathcal{PL}(\omega)$, which is formally stated in the following theorem.

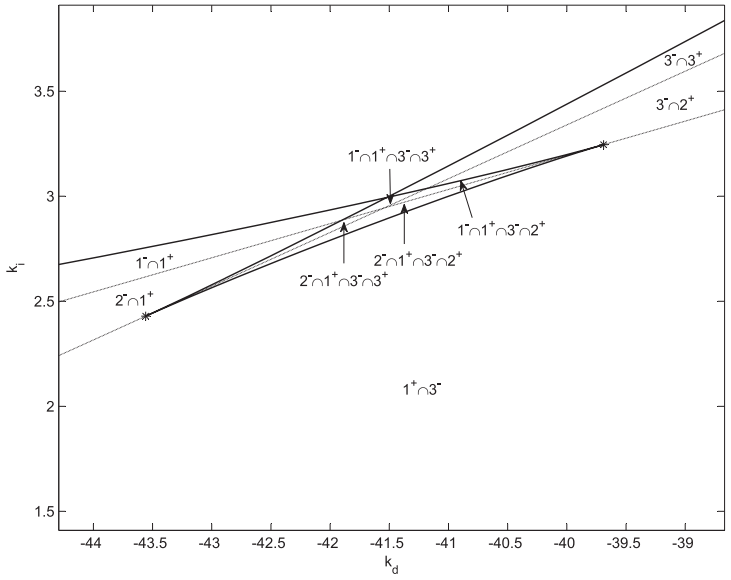

FIGURE 12 The regions of I

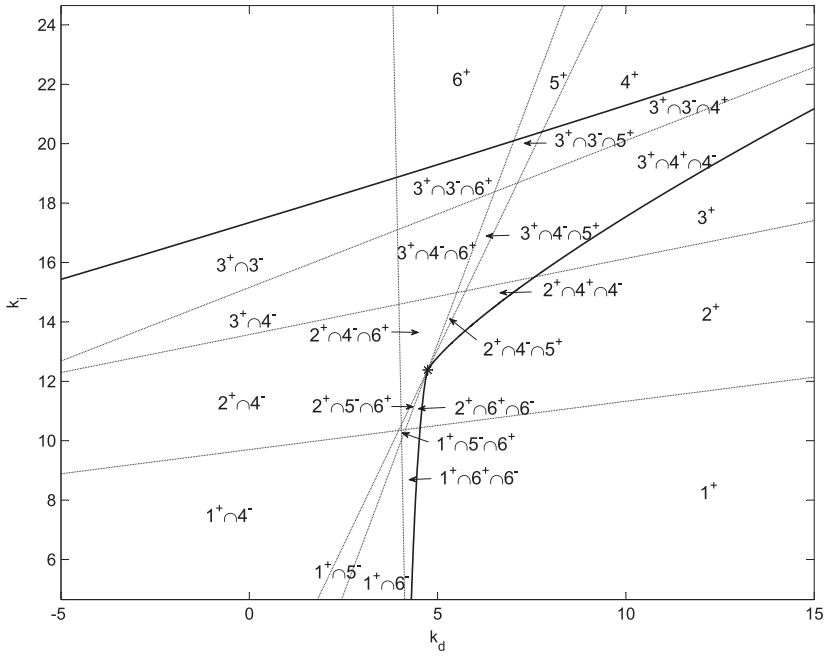

FIGURE 13 The regions of II

Theorem 1. *The surface S is completely determined by the discriminant D.*

Indeed, if D is given by (16), or in component form (17), (18), and (19), then it is necessary that

$$(k_i^d)'(\omega) = \omega^2 (k_d^d)'(\omega), \tag{23}$$

and S can be expressed as

$$k_d = k_d^d(\omega) + \gamma, \tag{24}$$

$$k_i = k_i^d(\omega) + \omega^2 \gamma, \tag{25}$$

$$k_p = k_p^d(\omega), \tag{26}$$

with $\omega \in (0, \infty)$ and $\gamma \in (-\infty, \infty)$.

FIGURE 14 The regions of III

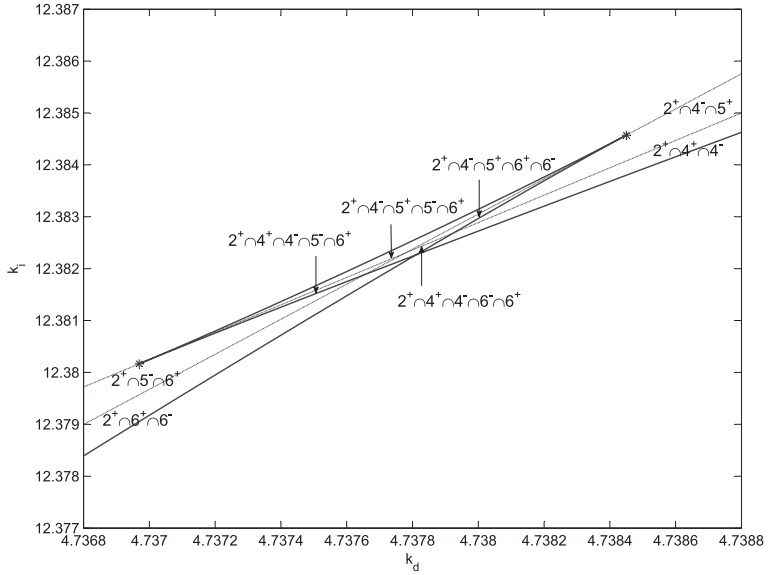

For a fixed ω, (24), (25), and (26) represent $\mathcal{L}(\omega)$ since (24) and (25) satisfy (5). It is useful to divide $\mathcal{L}(\omega)$ at the point $\mathbf{r}^d(\omega) = (k_d^d(\omega), k_i^d(\omega), k_p^d(\omega))$ into two parts

$$\mathcal{L}^+(\omega) = \{(k_d^d(\omega) + \gamma, k_i^d(\omega) + \omega^2\gamma, k_p^d(\omega))|\gamma > 0\},$$
$$\mathcal{L}^-(\omega) = \{(k_d^d(\omega) + \gamma, k_i^d(\omega) + \omega^2\gamma, k_p^d(\omega))|\gamma < 0\}.$$

Naturally, their projections on the (k_d, k_i) plane are denoted as $\mathcal{PL}^+(\omega)$ and $\mathcal{PL}^-(\omega)$, respectively.

4 | CUSPS AND PATCHES

In this section, we describe the cusps and patches. The points in the discriminant that violate the condition (22) play an important role in our analysis. To simplify our presentation, we make the following regularity assumption, which will be a standing assumption unless explicitly pointed out.

Assumption 2. No $\omega \in (0, \infty)$ may simultaneously satisfy

$$\phi(\omega) = \omega a''(\omega) - a'(\omega) = 0, \tag{27}$$

$$\phi'(\omega) = \omega a'''(\omega) = 0. \tag{28}$$

If $\phi(\omega^*) = 0$, then the above assumption means that $\phi(\omega)$ must have opposite signs for $\omega = \omega^* + \varepsilon$ and $\omega = \omega^* - \varepsilon$ when $\varepsilon > 0$ is sufficiently small, and $(k_d^d(\omega^*), k_i^d(\omega^*))$ is a cusp of $\mathcal{PD}$. This is obvious if we notice that $(k_d^d)'(\omega)$ and $(k_i^d)'(\omega)$ change sign at such a point. At a cusp, the tangent to $\mathcal{PD}$ may still be defined by its limit, and still has the slope ω^2. The tangent of the discriminant $\mathcal{D}$ at such a point is vertical if

$$\frac{dk_p^d}{d\omega} = \left[-\frac{b(\omega)}{\omega}\right]' \neq 0. \tag{29}$$

It is not too difficult to handle the irregular points that violate Assumption 2. For instance, let $\phi^{(k)}(\omega) = 0$ for $k = 0, 1, \ldots, m-1$, and $\phi^{(m)}(\omega) \neq 0$, then ω corresponds to a cusp if m is odd, but it is not a cusp if m is even, and the readers should not have difficulty generalizing the analysis in this article to such cases.

For the system with plant transfer function (10), $\mathcal{PD}$ has five cusps, and the corresponding ω are denoted as ω_i, $i = 1, 2, \ldots 5$. These cusps are also labeled in Figure 3.

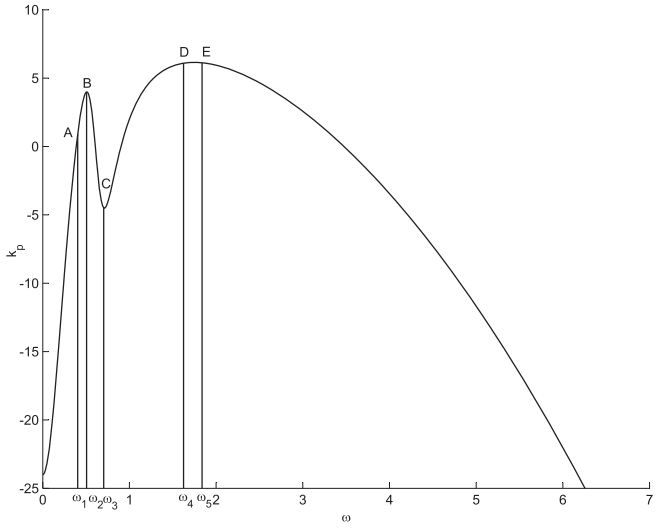

FIGURE 15 The change of k_p with ω

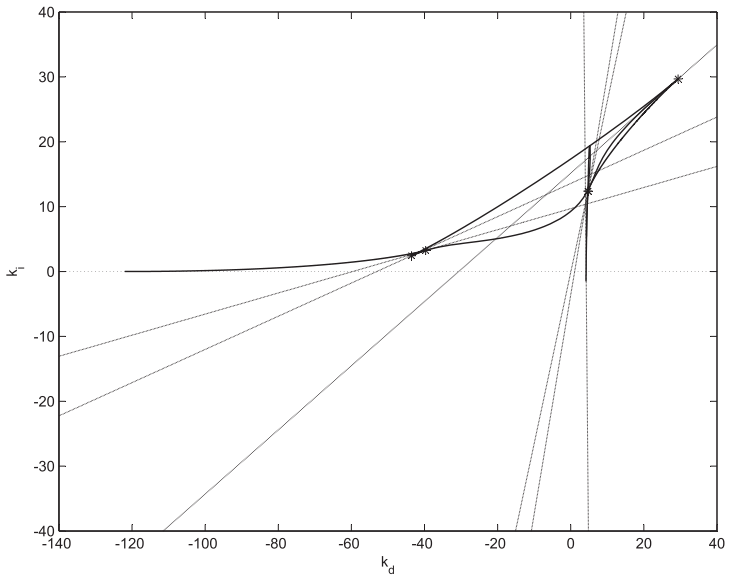

FIGURE 16 The intersection curve

Let ω_i, $i = 1, 2, \ldots, n-1$ corresponds to the cusps of $\mathcal{PD}$, and arranged in ascending order

$$\omega_1 < \omega_2 < \ldots < \omega_{n-1}.$$

They partition $(0, \infty)$ into n intervals Ω_i, $i = 1, 2, \ldots, n$,

$$\begin{aligned} \Omega_1 &= (0, \omega_1], \\ \Omega_i &= [\omega_{i-1}, \omega_i], \ i = 2, 3, \ldots, n-1, \\ \Omega_n &= [\omega_{n-1}, \infty). \end{aligned}$$

Correspondingly, we may partition the discriminant $\mathcal{D}$ into n sectors

$$\mathcal{D}_i = \{(k_d^d(\omega), k_i^d(\omega), k_p^d(\omega)) | \omega \in \Omega_i\}.$$

The projection of $\mathcal{D}_i$ on the (k_d, k_i) plane is denoted as $\mathcal{PD}_i$. Obviously, $\mathcal{PD}_i$, $i = 1, 2, \ldots, n$, partition $\mathcal{PD}$.

It is observed that the slope of the tangent of $\mathcal{PD}_i$ corresponding to ω is ω^2, which increases as one moves along $\mathcal{PD}_i$ in the directions of increasing ω, from which we may use the Theorem on Turning Tangent[14] to arrive at the following theorem.

FIGURE 17 Region I

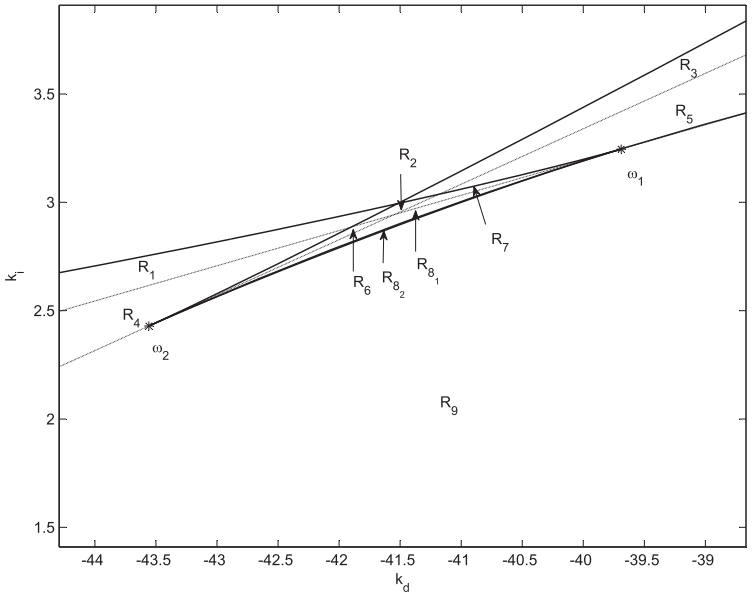

FIGURE 18 Zoom in on Region I

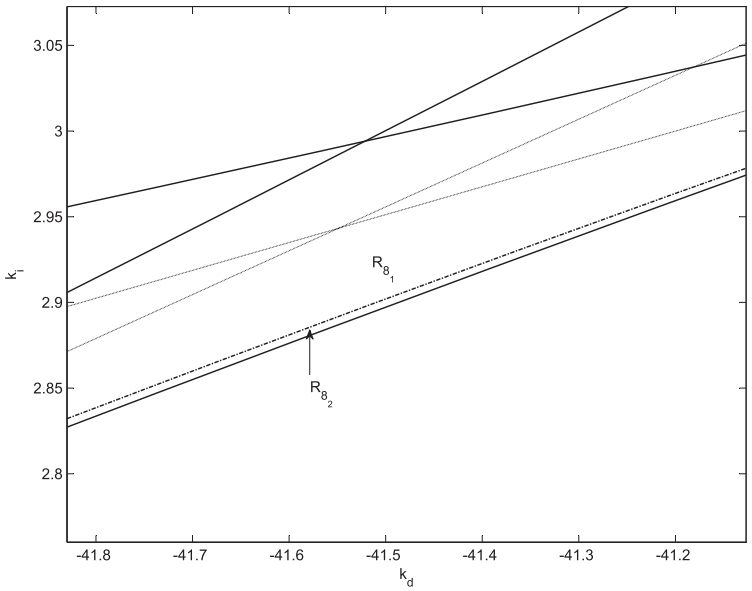

Theorem 2. *The center of curvature is always on the left hand side as one traverses $\mathcal{PD}_i$ along the direction of increasing ω. The region bounded by $\mathcal{PD}_i$ and the line segment connecting the two end points of $\mathcal{PD}_i$ is convex.*

We may also partition $\mathcal{S}$ into $2n$ patches

$$\mathcal{S}_i^+ = \{\mathcal{L}^+(\omega)|\omega \in \Omega_i\},$$
$$\mathcal{S}_i^- = \{\mathcal{L}^-(\omega)|\omega \in \Omega_i\}.$$

$\mathcal{S}_i^+$ is known as the ith positive patch, and $\mathcal{S}_i^-$ the ith negative patch. Their projections on the (k_d, k_i) plane are denoted as $\mathcal{PS}_i^+$ and $\mathcal{PS}_i^-$, respectively. An example of $\mathcal{PS}_i^+$ is shown in Figure 4. Figure 5 shows an example of and $\mathcal{PS}_i^-$.

Obviously, $\mathcal{D}_i$, $\mathcal{L}^+(\omega_{i-1})$, and $\mathcal{L}^+(\omega_i)$ form the boundary of $\mathcal{S}_i^+$, and $\mathcal{D}_i$, $\mathcal{L}^-(\omega_{i-1})$ and $\mathcal{L}^-(\omega_i)$ form the boundary of $\mathcal{S}_i^-$. When projected to the (k_d, k_i) plane, as illustrated in Figure 6, the sector $\mathcal{PD}_i$, the tangents $\mathcal{PL}^+(\omega_{i-1})$ and $\mathcal{PL}^+(\omega_i)$ divide the (k_d, k_i) plane into two regions $\mathcal{PS}_i^+$ and $(\mathcal{PS}_i^+)^c$. Similarly, $\mathcal{PD}_i$, $\mathcal{PL}^-(\omega_{i-1})$ and $\mathcal{PL}^-(\omega_i)$ divide the (k_d, k_i) plane into two regions $\mathcal{PS}_i^-$ and $(\mathcal{PS}_i^-)^c$ as shown in Figure 7. $\mathcal{PD}_i$, $P\mathcal{L}(\omega_{i-1})$, and $\mathcal{PL}(\omega_i)$ divide $\mathbb{R}^2$ into five regions as shown in Figure 8, $\mathcal{PS}_i^+ \cap (\mathcal{PS}_i^-)^c$, $\mathcal{PS}_i^+ \cap \mathcal{PS}_i^-$, $(\mathcal{PS}_i^+)^c \cap \mathcal{PS}_i^-$, and two components of $(\mathcal{PS}_i^+)^c \cap (\mathcal{PS}_i^-)^c$.

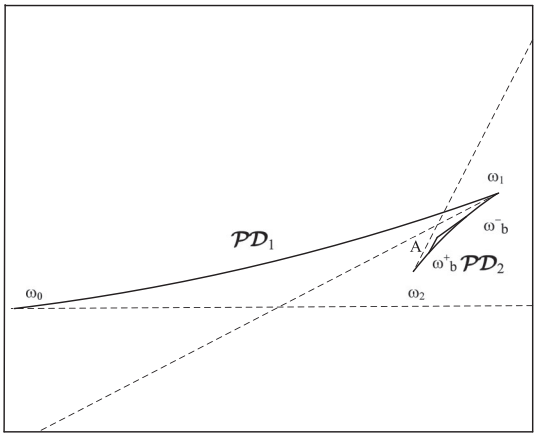

FIGURE 19 The illustration to judge the order of S_2^- and S_2^+

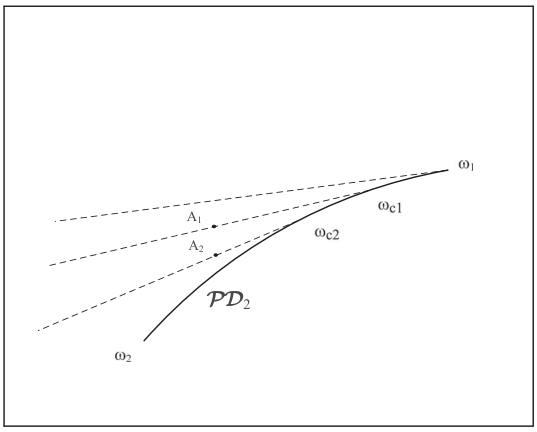

FIGURE 20 The illustration to show the change of S_2^-

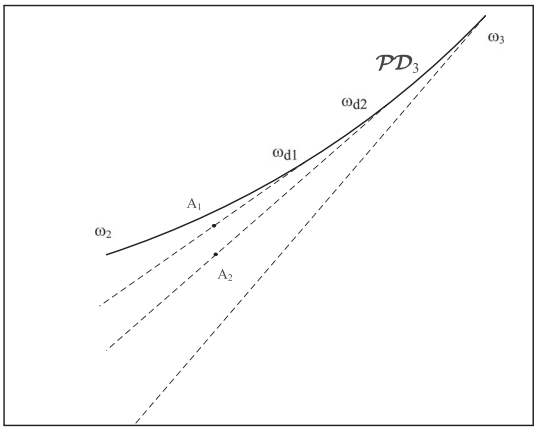

FIGURE 21 The illustration to show the change of S_3^-

A few comments on the first and last sectors are in order. The boundary of $S_1^{\pm}$ consists of D_1, $\mathcal{L}^{\pm}(0)$ and $\mathcal{L}^{\pm}(\omega_1)$, where $\mathcal{L}^{\pm}(0) = \lim_{\omega\to 0}\mathcal{L}^{\pm}(\omega)$, and the limits are well defined under Assumption 1. Therefore, $\mathcal{PL}^{\pm}(0)$ are also well defined, and the (k_d, k_i) plane can still be partitioned in Figure 8 for $i = 1$ with $\mathcal{PL}(\omega_0) = \mathcal{PL}(0)$ horizontal. For $S_n^{\pm}$, obviously, D_n and $\mathcal{L}^{\pm}(\omega_{n-1})$ form part of the boundary. However, the remaining piece of the boundary has a number of possibilities.

Case 1.

$$k_d^d(\infty) = \lim_{\omega\to\infty} k_d^d(\omega) = \text{finite}, \tag{30}$$

$$k_i^d(\infty) = \lim_{\omega\to\infty} k_i^d(\omega) = \text{finite}, \tag{31}$$

$$k_p^d(\infty) = \lim_{\omega\to\infty} k_p^d(\omega) = \text{finite}. \tag{32}$$

FIGURE 22 The orders of the layers

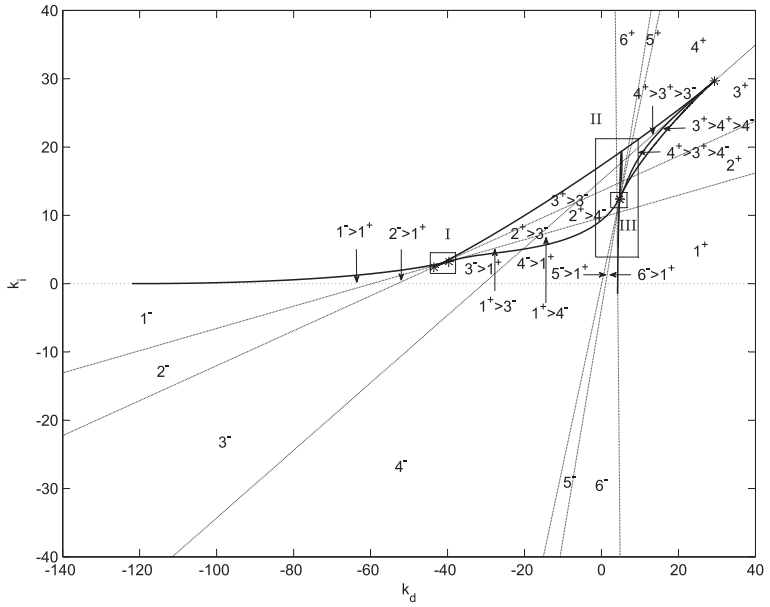

FIGURE 23 The orders of the layers in Region I

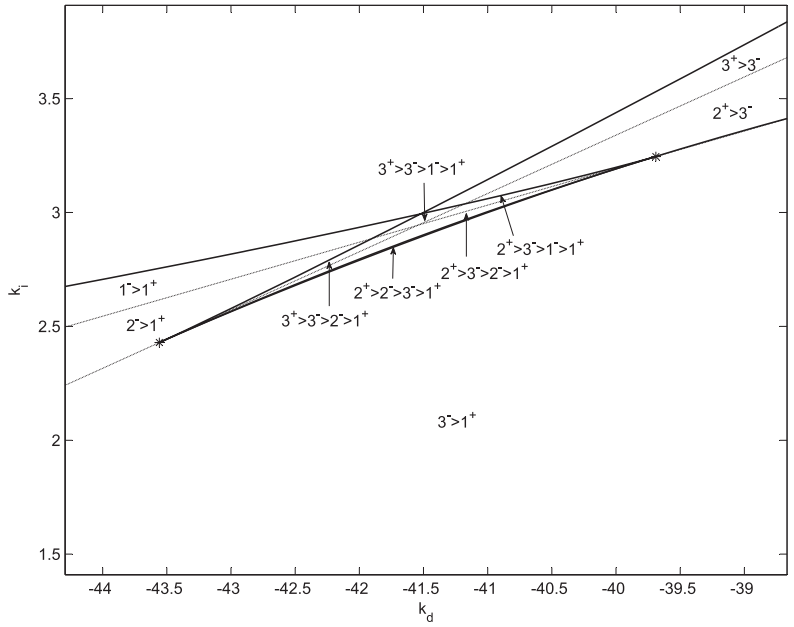

In this case, $\mathcal{L}^{\pm}(\omega_n) = \mathcal{L}^{\pm}(\infty)$ may be defined as

$$k_d = k_d^d(\infty), \tag{33}$$

$$k_i = k_i^d(\infty) \pm \alpha, \tag{34}$$

$$k_p = k_p^d(\infty), \tag{35}$$

with $\alpha \in (0, \infty)$, and form part of the boundary of $\mathcal{S}_n^{\pm}$. The projection on the (k_d, k_i) plane is still similar to Figure 8 for $i = n$ with $\mathcal{L}(\omega_n)$ vertical.

Case 2. (30) and (31) hold, but $\lim_{\omega\to\infty} k_p^d(\omega) = \pm\infty$. In this case, $\mathcal{L}(\infty)$ no longer exists as $\mathcal{S}_n^{\pm}$ approaches $\pm\infty$ in the k_p direction. However, $\mathcal{PL}^{\pm}(\infty) = \lim_{\omega\to\infty} \mathcal{PL}^{\pm}(\omega)$ can still be defined by (33) and (34), and form part of the bounding for $\mathcal{PS}_n^{\pm}$. The projection on the (k_d, k_i) plane is the same as in case 1.

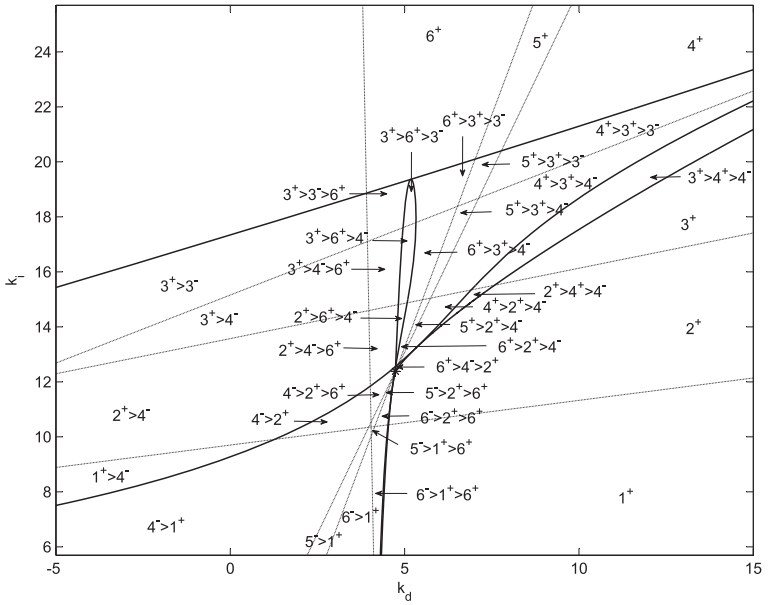

FIGURE 24 The orders of the layers in Region II

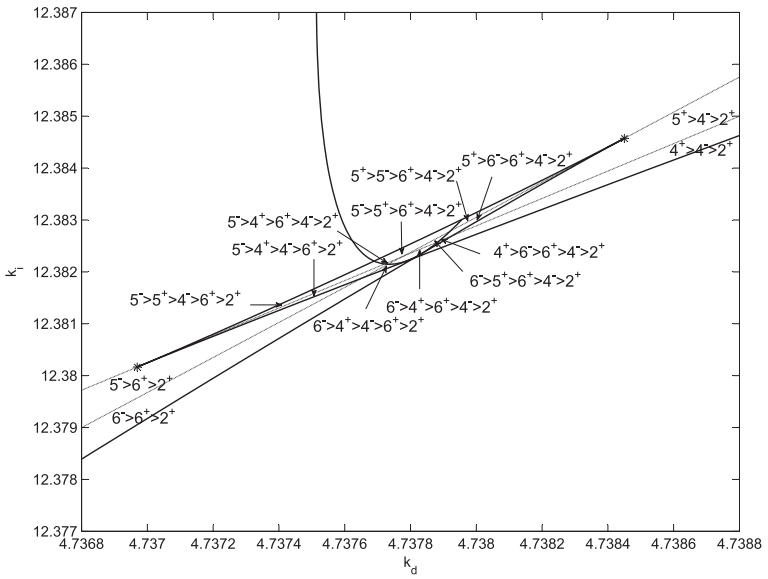

FIGURE 25 The orders of the layers in Region III

Case 3. (30) holds, but $k_i^d(\infty) = \infty$. In this case, $\mathcal{PL}^+(\infty)$ no longer exists, but $\mathcal{PL}^-(\infty)$ may be defined as (33) and

$$k_i = \alpha,\ \alpha \in (-\infty, \infty). \tag{36}$$

The situation may be illustrated in Figure 9.

Case 4. (30) holds, but $k_i^d(\infty) = -\infty$. In this case, $\mathcal{PL}^-(\infty)$ no longer exists, but $\mathcal{PL}^+(\infty)$ may be defined as (33) and (36).

Case 5. $\lim_{\omega\to\infty} k_d^d(\omega) = \pm\infty$. In this case, neither $\mathcal{PL}^+(\infty)$ nor $\mathcal{PL}^-(\infty)$ exists, and $\mathcal{PS}_n^{\pm}$ extend to ∞ or $-\infty$ in the k_d direction. The situation is illustrated in Figure 10 for the case of $k_d^d(\omega) \to +\infty$.

The five cases exhaust all the possibilities. Taken together, $\mathcal{PD}_i$, $i = 1, 2, \dots, n$; $\mathcal{PL}^{\pm}(0)$, $\mathcal{PL}^{\pm}(\omega_i)$, $i = 1, 2, \dots, n-1$, and possibly $\mathcal{PL}^{\pm}(\infty)$ when applicable, partition the (k_d, k_i) plane into open regions. Denote these regions as R_k, $k = 1, 2, \dots, N$,

$$\mathrm{cl}\left(\bigcup_{k=1}^{N} R_k\right) = \mathbb{R}^2,\ R_k \cap R_l = \emptyset,$$

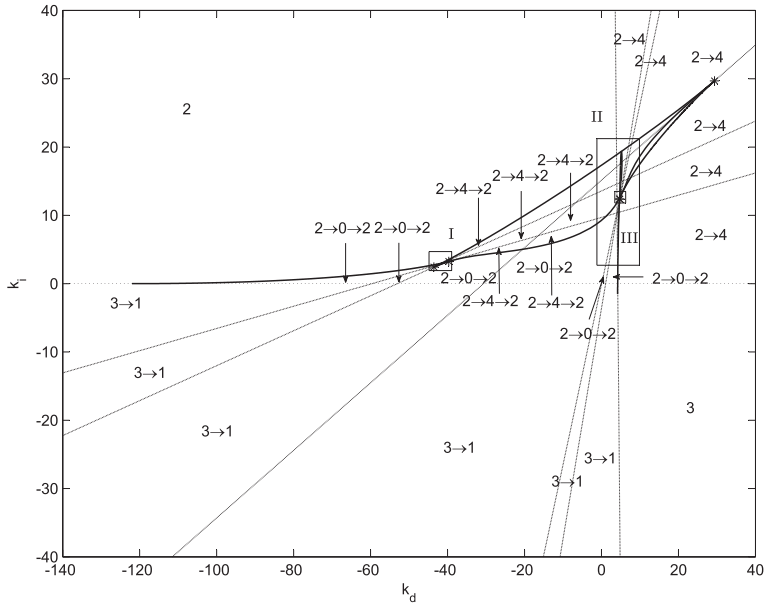

FIGURE 26 The change of the roots on right half-plane

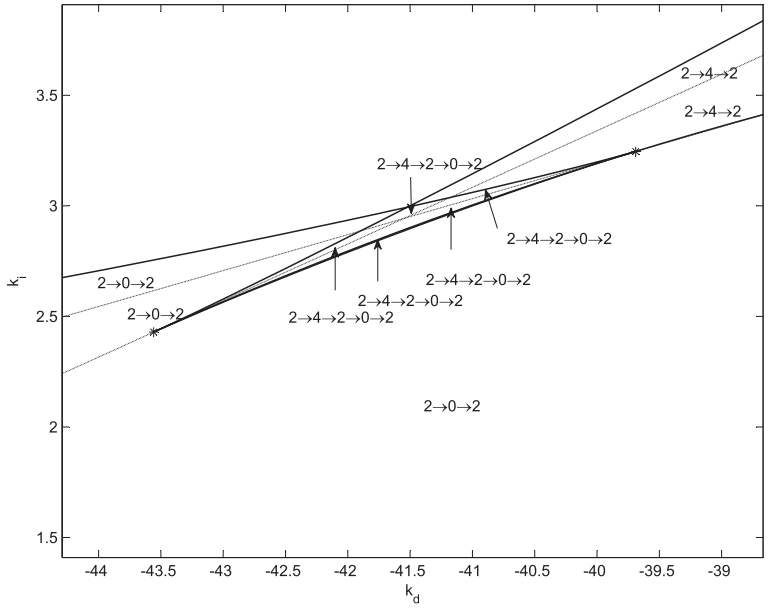

FIGURE 27 The change of the roots on right half-plane of Region I

where cl is the closure operator on a set. Consider a given region R_k. As it does not contain the boundary of $\mathcal{PS}_i^+$ or $\mathcal{PS}_j^-$, we may associate R_k with a pair of index sets $\mathcal{I}_k^+ \subset \mathbb{N}_n$, $\mathcal{I}_k^- \subset \mathbb{N}_n$, where $\mathbb{N}_n = \{1, 2, \dots, n\}$. For each point $\mathbf{r} = (k_d, k_i) \in R_k$, $\mathbf{r} \in \mathcal{PS}_i^+$ or $\mathbf{r} \in \mathcal{PS}_j^-$ if and only if $i \in \mathcal{I}_k^+$ or $j \in \mathcal{I}_k^-$, respectively.

Let $\mathcal{I}_k^+ = \{i_1, i_2, \dots, i_l\}$, $\mathcal{I}_k^- = \{j_1, j_2, \dots, j_m\}$, and represent these two index sets by a single set

$$\mathcal{I}_k = \left\{i_1^+, i_2^+, \dots, i_l^+, j_1^-, j_2^-, \dots, j_m^-\right\} \subset \mathbb{N}_n^{\pm}, \tag{37}$$

where $\mathbb{N}_n^{\pm} = \{1^+, 2^+, \dots, n^+, 1^-, 2^-, \dots, n^-\}$. Such a notation also allows us to use the same notation $\mathcal{S}_\alpha$ to represent positive and negative patches,

$$\mathcal{S}_\alpha = \begin{cases} \mathcal{S}_i^+ & \text{if } \alpha = i^+, \\ \mathcal{S}_j^- & \text{if } \alpha = j^-. \end{cases}$$

The same can be done for $\mathcal{PS}_i^+$ and $\mathcal{PS}_i^-$. Then the above can be summarized in the following theorem.

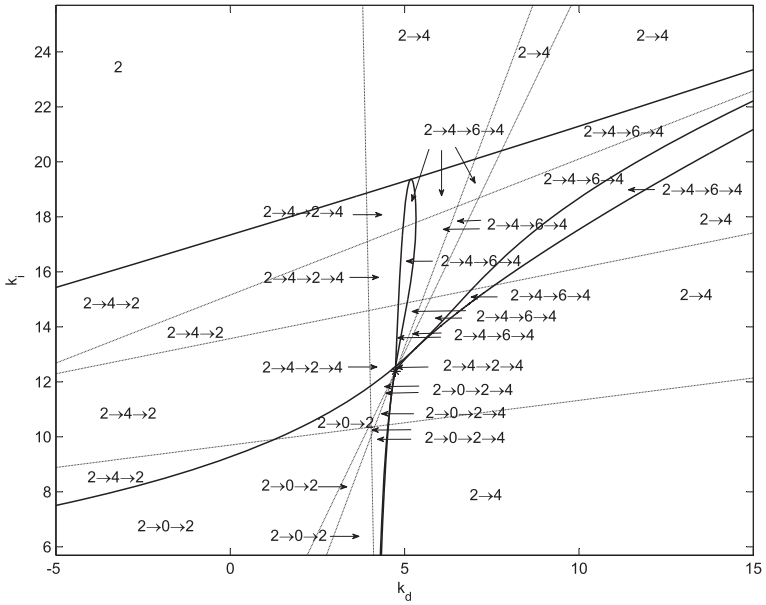

FIGURE 28 The change of the roots on right half-plane of Region II

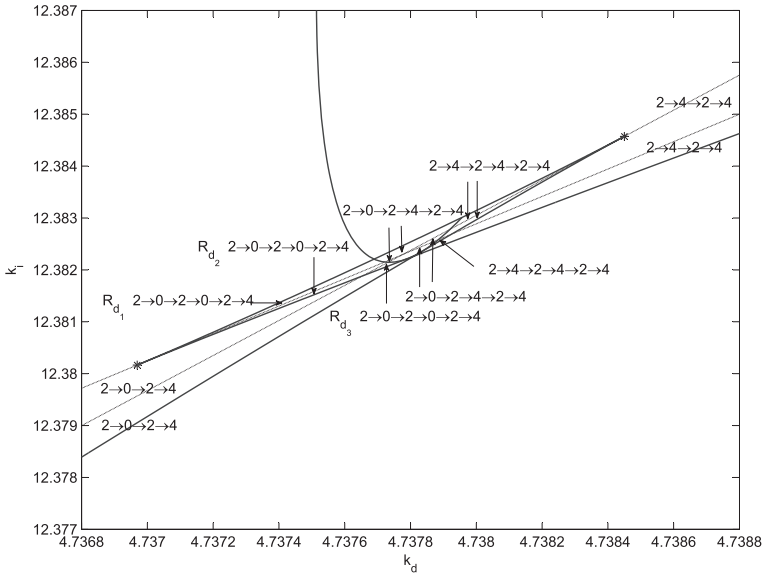

FIGURE 29 The change of the roots on right half-plane of Region III

Theorem 3. *For $\mathcal{I}_k$ defined above, one has*

$$
\begin{aligned}
&R_k \subset \mathcal{PS}_\alpha,\ \alpha \in \mathcal{I}_k,\\
&R_k \cap \mathcal{PS}_\alpha = \emptyset,\ \alpha \notin \mathcal{I}_k,\\
&R_k \subset \left(\bigcap_{\alpha\in\mathcal{I}_k} \mathcal{PS}_\alpha\right) \cap \left(\bigcup_{\beta\in\mathbb{N}_n^{\pm}\setminus\mathcal{I}_k} (\mathcal{PS}_\beta)^c\right).
\end{aligned}
$$

For the system with plant transfer function (10), the partition of the (k_d, k_i) plane with the corresponding index sets is given in Figure 11 with amplified view of three regions given in Figures 12–14. In the figures, a region $\mathcal{R}_k$ with index set $\mathcal{I}_k$ given in (37) is labeled as $i_1^+ \cap i_2^+ \cap \ldots \cap i_l^+ \cap j_1^- \cap j_2^- \cap \ldots \cap j_m^-$. Given any point $(k_d^*, k_i^*) \in \mathcal{R}_k$, the vertical

$$
\mathcal{VL}(k_d^*, k_i^*) = \left\{(k_d^*, k_i^*, k_p) | -\infty < k_p < \infty\right\}
$$

intersects with all patches $\mathcal{S}_\alpha$, $\alpha \in \mathcal{I}_k$, but does not intersect with any patch $\mathcal{S}_\beta$, $\beta \notin \mathcal{I}_k$.

5 | RELATIVE VERTICAL POSITIONS OF PATCHES

In this section, we discuss how to determine the relative vertical positions of patches. The knowledge of the relative vertical positions, along with the crossing directions of patches (to be discussed in the next section) will allow us to determine the number of roots on the RHP for each parameter region.

$$k_p(\omega_1) = k_p(\omega_2). \tag{38}$$

For a given point $(k_d, k_i) \in \mathcal{R}_k$, let the intersection of $\mathcal{VL}(k_d, k_i)$ and $\mathcal{S}_\alpha$ be $(k_d, k_i, k_{p\alpha})$. Assume

$$k_{p\alpha} \neq k_{p\beta}, \text{ whenever } \alpha \neq \beta.$$

Then, we can order the elements of the index set I_k as $\alpha_1, \alpha_2, \ldots, \alpha_{l+m}$, such that

$$k_{p\alpha_1} > k_{p\alpha_2} > \ldots > k_{p\alpha_{l+m}}.$$

In this case, we write, at (k_d, k_i),

$$\mathcal{S}_{\alpha_1} > \mathcal{S}_{\alpha_2} > \ldots > \mathcal{S}_{\alpha_{l+m}}. \tag{39}$$

In general, the order is different for different $(k_d, k_i) \in \mathcal{R}_k$. For a complete stability analysis, we want to further partition $\mathcal{R}_k$ into subregions $\mathcal{R}_{k_i}$, $i = 1, 2, \ldots, m_k$, such that the order (39) is independent of (k_d, k_i) as long as it is within the subregion $\mathcal{R}_{k_i}$. The internal boundaries that divide $\mathcal{R}_k$ into these subregions are the intersections between the patches projected on the (k_d, k_i) plane. Such boundaries can be obtained by considering the k_p versus ω relation. Recall that for the plant transfer function given by (10), the relation is given in Figure 15. Let $\omega_1 \neq \omega_2$, satisfy

$$k_p(\omega_1) = k_p(\omega_2). \tag{40}$$

Then $\mathcal{L}(\omega_1)$ intersects $\mathcal{L}(\omega_2)$. The intersection can be obtained by requiring (k_d, k_i) to satisfy (5) for $\omega = \omega_1$, and $\omega = \omega_2$. The resulting two equations can be solved to obtain

$$k_d = \frac{a(\omega_2) - a(\omega_1)}{\omega_2^2 - \omega_1^2}, \tag{41}$$

$$k_i = \frac{\omega_1^2 a(\omega_2) - \omega_2^2 a(\omega_1)}{\omega_2^2 - \omega_1^2}. \tag{42}$$

The collection of all (ω_1, ω_2) that satisfy (40) corresponds to all the intersections between different patches. Notice, given an ω_1, all the possible ω_2 to satisfy (40) can be easily solved numerically as (40) can be written as a polynomial equation of ω_2. For the system with plant transfer function (10), Figure 16 shows all the intersections in addition to all the $\mathcal{PD}_i$ and $\mathcal{PL}(\omega_i)$ given in Figure 11. Figures 17 and 18 give amplified views. Within each $\mathcal{R}_{k_i}$, we may order the index set $\mathcal{I}_k$ such that (39) is true for all $(k_d, k_i) \in \mathcal{R}_{k_i}$. (39) may be interpreted as $\mathcal{S}_{\alpha_1}$ above $\mathcal{S}_{\alpha_2}$, which in turn is above $\mathcal{S}_{\alpha_3}$, and so on. Within the column

$$\left\{ \mathcal{VL}(k_d, k_i) | (k_d, k_i) \in \mathcal{R}_{k_i} \right\},$$

for any (k_d, k_i, k_p) in the region between $\mathcal{S}_{\alpha_j}$ and $\mathcal{S}_{\alpha_{j+1}}$, the characteristic equation has a fixed number of roots on the right half complex plane. This is also true for the region above $\mathcal{S}_{\alpha_1}$ and below $\mathcal{S}_{\alpha_{l+m}}$.

We now discuss how to determine the relative vertical positions of $\mathcal{S}_\alpha$, $\alpha \in \mathcal{I}_k$ within each $\mathcal{R}_{k_i}$. We need to only choose an arbitrary $(k_d^*, k_i^*) \in \mathcal{R}_{k_i}$ to determine this order as it does not change within $\mathcal{R}_{k_i}$. This can be carried out as follows: For each $\alpha \in \mathcal{I}_k$, if $\mathcal{S}_\alpha$ is a positive patch, say S_j^+, then we may determine the unique $\omega_\alpha \in (\omega_{j-1}, \omega_j)$ such that $(k_d^*, k_i^*) \in \mathcal{PL}^+(\omega_\alpha)$. If $\mathcal{S}_\alpha$ is a negative patch, then we need $(k_d^*, k_i^*) \in \mathcal{PL}^-(\omega_\alpha)$ instead. Geometrically, this means drawing a tangent of $\mathcal{PD}_i$ that passes through the point (k_d^*, k_i^*), and the point (k_d^*, k_i^*) is on the right of the tangent point if it is a positive patch,

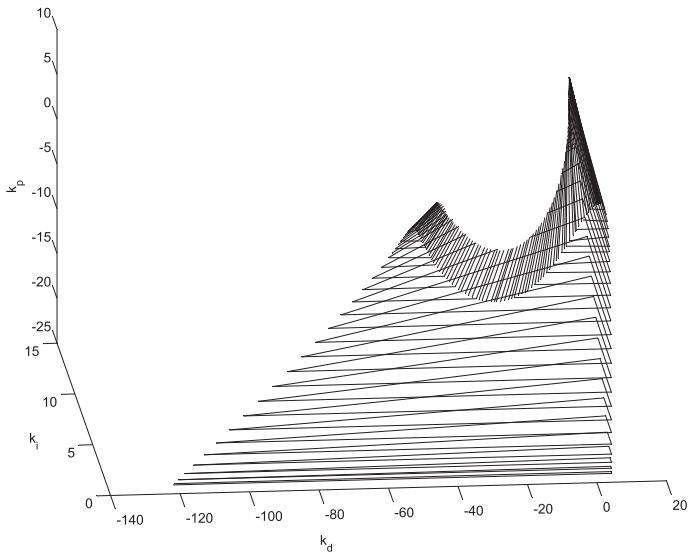

FIGURE 30 The stable regions (angle1).

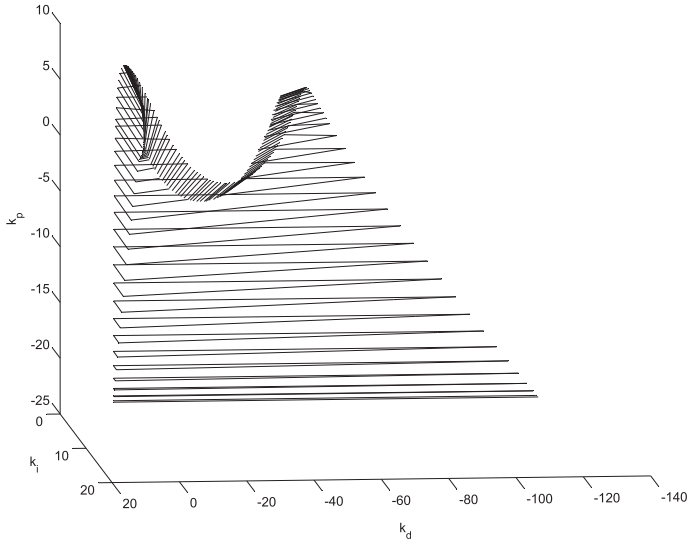

FIGURE 31 The stable regions (angle2)

and it is on the left if it is a negative patch. ω_α can be easily be determined numerically. Indeed, $\mathcal{PL}(\omega_\alpha)$ must satisfy (5) for $k_d = k_d^*$, $k_i = k_i^*$, and $\omega = \omega_\alpha$. As k_d^* and k_i^* are given, (5) may be written as a polynomial equation of ω. The applicable solution ω_α needs to be real and satisfy $\omega_\alpha \in (\omega_{j-1}, \omega_j)$ and $k_d^d(\omega_\alpha) < k_d^*$ (if $\mathcal{S}_\alpha$ is a positive patch) or $k_d^d(\omega_\alpha) > k_d^*$ (if $\mathcal{S}_\alpha$ is a negative patch). Corresponding to the $l+m$ elements of the index set $\mathcal{I}_k$, $\alpha_1, \alpha_2, \ldots, \alpha_{l+m}$, we may find $\omega_{\alpha_1}, \omega_{\alpha_2}, \ldots, \omega_{\alpha_{l+m}}$. They should be arranged in a order so that

$$k_p(\omega_{\alpha_1}) > k_p(\omega_{\alpha_2}) > \ldots > k_p(\omega_{\alpha_{l+m}}).$$

As a result, the patches satisfy

$$\mathcal{S}_{\alpha_1} > \mathcal{S}_{\alpha_2} > \ldots > \mathcal{S}_{\alpha_{l+m}}.$$

in $\mathcal{R}_{k_i}$.

We will use $\mathcal{R}_8$ shown in Figure 17 and amplified view in Figure 18 as an example on how to make judgement about the relative vertical positions of the patches. It is known that $\mathcal{I}_8 = \{1^+, 2^+, 2^-, 3^-\}$, and is divided by the intersection between 2^- and 3^- into two subregions $\mathcal{R}_{8_1}$ and $\mathcal{R}_{8_2}$. As ω increases, $\mathcal{PD}_1$ and $\mathcal{PD}_3$ move to the right, and $\mathcal{PD}_2$ moves to the left. From Figure 15, it is obvious that for any $\omega_a \in (0, \omega_1)$, $\omega_b \in (\omega_1, \omega_2)$, $k_p(\omega_b) > k_p(\omega_a)$, from which we conclude $\mathcal{S}_2^+ > \mathcal{S}_1^+$, $\mathcal{S}_2^- > \mathcal{S}_1^+$. $\mathcal{S}_3^- > \mathcal{S}_1^+$ can be judged similarly. As shown in Figure 19, drawing tangents from a point A in $\mathcal{R}_8$ to

FIGURE 32 The stable regions (angle3)

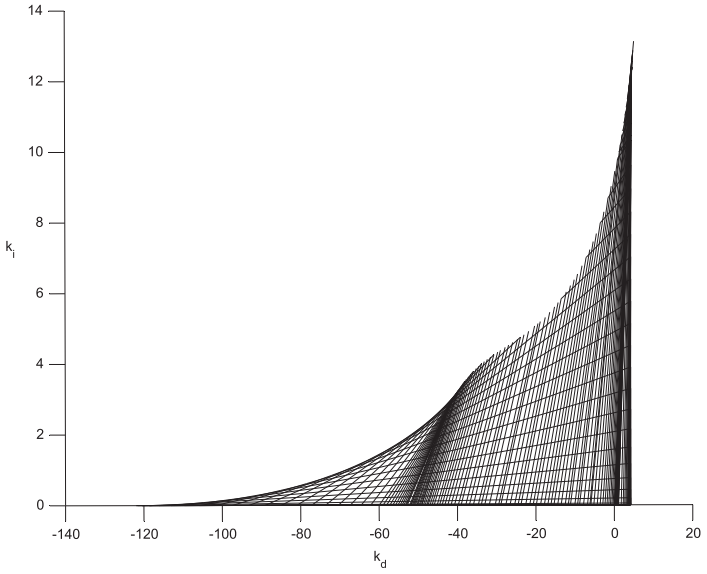

FIGURE 33 The stable regions of Region III (angle1)

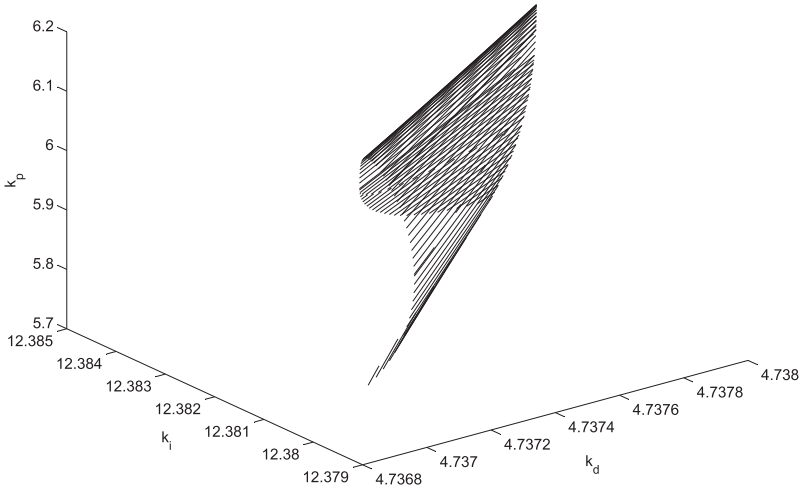

$\mathcal{PD}_2$, and let the tangent points correspond to ω_b^+ and ω_b^-, such that A is on $\mathcal{PL}^+(\omega_b^+)$ and $\mathcal{PL}^-(\omega_b^-)$. Then the tangent point of $\mathcal{PL}^-(\omega_b^-)$ is on the right of that of $\mathcal{PL}^+(\omega_b^+)$. Therefore, $\omega_b^+ > \omega_b^-$, from which and Figure 15 we conclude that $S_2^+ > S_2^-$. Now consider moving A from A_1 to A_2 (further away from $\mathcal{PD}_3$ and closer to $\mathcal{PD}_2$). As shown in Figures 20 and 21, let the tangent points corresponded to ω_{c_1} and ω_{c_2} in $\mathcal{PD}_2$, and ω_{d_1} and ω_{d_2} in $\mathcal{PD}_3$, respectively. It is obvious that $\omega_{c_2} > \omega_{c_1}$ and $\omega_{d_2} > \omega_{d_1}$. From Figure 15, one has $k_p(\omega_{c_2}) > k_p(\omega_{c_1})$ and $k_p(\omega_{d_2}) < k_p(\omega_{d_1})$. Therefore, as A moves from A_1 to A_2 crossing the intersection between S_2^- and S_3^-, $S_2^- < S_3^-$ is changed to $S_2^- > S_3^-$. From the above analysis, we conclude that

$$S_2^+ > S_3^- > S_2^- > S_1^+ \quad \text{in } \mathcal{R}_{8_1},$$
$$S_2^+ > S_2^- > S_3^- > S_1^+ \quad \text{in } \mathcal{R}_{8_2}.$$

Of course, the more accurate numerical methods can be used to verify the above. The complete ordering of patches in all the subregions for the system with the plant transfer function (10) is given in Figures 22–25. In the figures,

$$S_{\alpha_1} > S_{\alpha_2} > \ \ldots \ > S_{\alpha_{l+m}},$$

is denoted as

$$\alpha_1 > \alpha_2 > \ \ldots \ > \alpha_{l+m}.$$

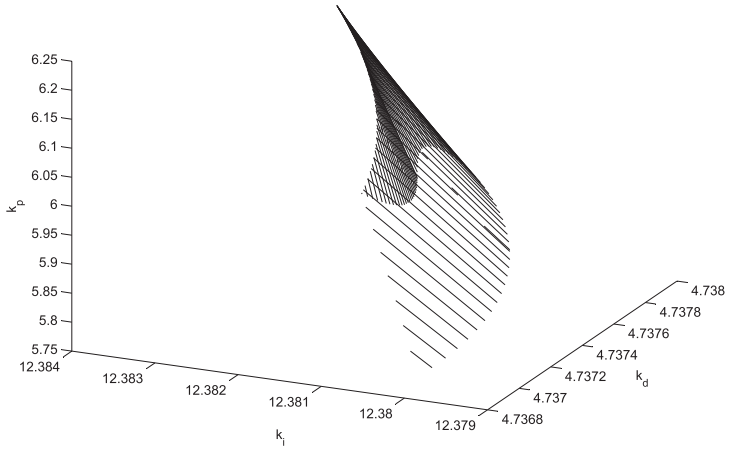

FIGURE 34 The stable regions of Region III (angle2)

6 | CROSSING DIRECTIONS

This section discusses the crossing directions. For each region in the (k_d, k_i) plane, there are several patches above it. By considering the vertical crossing direction, the change of the RHP roots can be determined as a point crosses the patch. In general, a pair of imaginary roots of the characteristic polynomial cross the imaginary axis as point (k_d, k_i, k_p) moves from one side of surface S to the other side. It turns out that when we move the parameter along the vertical direction, the crossing direction is very easy to judge.

Theorem 4. *As the parameters (k_d, k_i, k_p) moves across a positive patch along the $\mathcal{VL}(k_d, k_i)$ in the increasing k_p direction, two roots of the characteristic equation (2) cross the imaginary axis from RHP to LHP. The crossing of the characteristic roots is in the opposite direction if it is a negative patch.*

Proof. The characteristic equation (2) can be written as

$$G(s) + sk_p + k_i + s^2 k_d = 0, \tag{43}$$

where

$$G(s) = \frac{s}{G_p(s)}. \tag{44}$$

Taking derivative with respect to k_p using the implicit function theorem gives

$$G'(s)\frac{\partial s}{\partial k_p} + s + k_p\frac{\partial s}{\partial k_p} + 2sk_d\frac{\partial s}{\partial k_p} = 0, \tag{45}$$

which may be solved to yield

$$\frac{\partial s}{\partial k_p} = -\frac{s}{G'(s) + k_p + 2sk_d}. \tag{46}$$

From (44), (7), (8), we can take derivative to obtain

$$G'(s)|_{s=\omega j} = b'(\omega) - ja'(\omega). \tag{47}$$

A substitution of (46) by (47) yields

$$\left.\frac{\partial s}{\partial k_p}\right|_{s=\omega j} = -\frac{(2\omega k_d - a'(\omega))\omega - j\omega(b'(\omega) + k_p)}{(b'(\omega) + k_p)^2 + (2\omega k_d - a'(\omega))^2}. \tag{48}$$

Accordingly,

$$\mathrm{Re}\left(\left.\frac{\partial s}{\partial k_p}\right|_{s=\omega j}\right) = -\frac{\omega(2\omega k_d - a'(\omega))}{(b'(\omega) + k_p)^2 + (2\omega k_d - a'(\omega))^2}. \tag{49}$$

On a positive patch,

$$k_d > k_d^d = \frac{a'(\omega)}{2\omega}, \tag{50}$$

and therefore,

$$\mathrm{Re}\left(\frac{\partial s}{\partial k_p}\bigg|_{s=\omega j} \right) < 0. \tag{51}$$

By symmetry, we also have

$$\mathrm{Re}\left(\frac{\partial s}{\partial k_p}\bigg|_{s=-\omega j} \right) < 0. \tag{52}$$

(51) and (52) mean that a pair of complex conjugate roots cross the imaginary axis at $\pm\omega_j$ from the RHP to the left half plane as k_p increases across a positive patch.

Similarly, on a negative patch,

$$k_d < \frac{a'(\omega)}{2\omega}, \tag{53}$$

which yields

$$\mathrm{Re}\left(\frac{\partial s}{\partial k_p}\bigg|_{s=\omega j} \right) > 0, \tag{54}$$

and a pair of roots cross the imaginary axis from LHP to RHP. The proof is complete. ■

With the knowledge of the crossing direction and the vertical relative position of each region R_{ki}, we only need the number of RHP roots at one point in the parameter space to determine the number of RHP roots in each region. For one point with the known RHP roots, we can judge the crossing direction when this point crosses the surface $\mathcal{S}$ vertically. Then, the change of the number of the RHP roots is obtained. Finally, we can identify the set of stabilizing parameters.

For the system with plant transfer function (10), we can easily calculate that the system has two characteristic roots on the RHP when $k_i > 0$ and k_p is sufficiently large (above all the patches, $k_p > 7$ would be sufficient in view of Figure 15). It has three RHP roots when $k_i < 0$ and k_p is large. The difference is due to crossing of $\mathcal{V}$.

Consider now (k_d, k_i) is in the region $\mathcal{R}_2$ in Figure 17. From Figure 23, the relative vertical positions of the patches are

$$\mathcal{S}_3^+ > \mathcal{S}_3^- > \mathcal{S}_1^- > \mathcal{S}_1^+. \tag{55}$$

We already know that Equation (2) has two RHP roots when (k_d, k_i, k_p) is in the region above $\mathcal{S}_3^+$. As $\mathcal{S}_3^+$ is a positive patch, we can conclude from Theorem 2 that (2) has four RHP roots when the parameters are in the region between $\mathcal{S}_3^-$ and $\mathcal{S}_3^+$ (two more than above $\mathcal{S}_3^+$ because we need to cross $\mathcal{S}_3^+$ in the negative k_p direction in order to reach from the region above $\mathcal{S}_3^+$ to this region). As $\mathcal{S}_3^-$ is a negative patch, we can similarly use Theorem 2 to determine that (2) has two RHP roots when (k_d, k_i, k_p) is in the region between $\mathcal{S}_3^-$ and $\mathcal{S}_1^-$ (two less than the region above) and (2) has no RHP root when (k_d, k_i, k_p) is between $\mathcal{S}_1^-$ and $\mathcal{S}_1^+$, and it has two RHP roots when (k_d, k_i, k_p) is below $\mathcal{S}_1^+$. This is shown in Figure 27 as $2 \to 4 \to 2 \to 0 \to 2$. The same process can be applied to all the regions $\mathcal{R}_{k_i}$, and the results is shown in Figures 26–29. The collection of all the regions labeled as "0" is the stabilizing set. This stabilizing set is shown in three views in Figures 30,31,32. Two more detailed three-dimensional views for region III are given in Figures 33 and 34. Note that there are two layers of stable regions in this region.

7 | CONCLUSIONS

A geometric description of the et of all stabilizing PID controllers has been developed. The three-dimensional parameter space is partitioned by the stability crossing surface into regions such that the number of characteristic roots on the RHP

remains constant within each region. The stability crossing surface is a ruled surface, and it is completely determined by a curve known as the discriminant. The discriminant may be divided into sectors between its cusps, and each sector corresponds to a positive patch and a negative patch. The stability crossing surface is composed of these patches. The projection of the boundary of these patches to the horizontal plane formed by the derivative and integral coefficients allows us to partition this plane into regions such that there are a fixed number of patches in each such region, and these patches are in the same vertical order. By identifying the crossing directions, we may determine the number of RHP characteristic roots between any two patches. This allows us to obtain the regions in the plane where there are stabilizing proportional coefficient, and the corresponding pair of patches such that the system is stable when the proportional coefficient is between these pair of patches. The process is made easier by the knowledge that the crossing direction is the same for all the positive patches, and it is the opposite for all the negative patches.

ACKNOWLEDGEMENTS

Qian Ma was partially supported by National Science Foundation of China under Grant 61773207, and the Natural Science Fund for Distinguished Young Scholars of Jiangsu Province under Grant BK20190020 in this work.

DATA AVAILABILITY STATEMENT

The data that support the findings of this study are available from the corresponding author upon reasonable request.

ORCID

Qian Ma https://orcid.org/0000-0002-0593-0157

REFERENCES

1. Bazanella A, Pereira L, Parraga A. A new method for PID tuning including plants without ultimate frequency. *IEEE Trans Control Syst Technol*. 2017;25(2):637-644.
2. Boyd S, Hast M, Astrom K. MIMO PID tuning via iterated LMI restriction. *Int J Robust Nonliear Control*. 2016;26:1718-1731.
3. Ho W, Hang C, Cao L. Tuning of PID controllers based on gain and phase margin specifications. *Automatica*. 1995;31(3):497-502.
4. Meza J, Santibanez V, Soto R, Llama M. Fuzzy self-tuning PID semiglobal regulator for robot manipulators. *IEEE Trans Ind Electron*. 2012;59(6):2709-2717.
5. Zhang M, Borja P, Ortega R, Liu Z, Su H. PID passivity-based control of port-Hamiltonian systems. *IEEE Trans Autom Control*. 2018;63(4):1032-1044.
6. Soylemez M, Munro N, Baki H. Fast calculation of stabilizing PID controllers. *Automatica*. 2003;39(1):121-126.
7. Ho M, Datta A, Bhattacharyya S. A new approach to feedback stabilization. Paper presented at: Proceedings of the Conference on Decision and Control; December, 1996; Kobe, Japan.
8. Ho M, Datta A, Bhattacharyya S. A linear programming characterization of all stabilizing PID controllers. Paper presented at: Proceeding of the American Control Conference; June 1997; Albuquerque, New Mexico.
9. Ho M, Datta A, Bhattacharyya S. Control system design using low order controllers: constant gain, PI and PID. Paper presented at: Proceeding of the American Control Conference; June 1997; Albuquerque, New Mexico.
10. Ackermann J, Kaesbauer D. Stable polyhedra in parameter space. *Automatica*. 2003;39(5):937-943.
11. Wang D. Further results on the synthesis of PID controllers. *IEEE Trans Autom Control*. 2007;52(6):1127-1132.
12. Gu K, Ma Q, Zhou H, Mahzoon S, Yang X. A geometric description of the set of stabilizing PID controllers. Paper presented at: Proceeding of the 21th World Congress of the International Federation of Automatic Control; July 12-17, 2020; Berlin, Germany.
13. Guggenheimer H. *Differential Geometry*. New York, NY: Dover; 1977.
14. Chern SS, ed. *Studies in Global Geometry and Analysis*. Upper Saddle River, NJ: Prentice-Hall; 1967.

How to cite this article: Gu K, Ma Q, Zhou H, Mahzoon S, Yang X. A geometric description of the set of stabilizing PID controllers. *Int J Robust Nonlinear Control*. 2021;1–22. https://doi.org/10.1002/rnc.5443